Biomedical Research (Tokyo) **42** (4) 129–138, 2021

CLN6's luminal tail-mediated functional interference between CLN6 mutants as a novel pathomechanism for the neuronal ceroid lipofuscinoses

Yuki Shiro, Arisa Yamashita, Kana Watanabe, and Tetsuo Yamazaki
Department of Molecular Cell Biology and Medicine, Graduate School of Biomedical Sciences, Tokushima University, 1-78-1, Sho-machi, Tokushima 770-8505, Japan

(Received 5 April 2021; and accepted 25 May 2021)

ABSTRACT

CLN6 (Ceroid Lipofuscinosis, Neuronal, 6) is a 311-amino acid protein spanning the endoplasmic reticulum membrane. Mutations in *CLN6* are linked to CLN6 disease, a hereditary neurodegenerative disorder categorized into the neuronal ceroid lipofuscinoses. CLN6 disease is an autosomal recessive disorder and individuals affected with this disease have two identical (homozygous) or two distinct (compound heterozygous) *CLN6* mutant alleles. Little has been known about CLN6's physiological roles and the disease mechanism. We recently found that CLN6 prevents protein aggregate formation, pointing to impaired CLN6's anti-aggregate activity as a cause for the disease. To comprehensively understand the pathomechanism, overall anti-aggregate activity derived from two different CLN6 mutants needs to be investigated, considering patients compound heterozygous for CLN6 alleles. We focused on mutant combinations involving the S132CfsX18 (132fsX) prematurely terminated protein, produced from the most frequent mutation in *CLN6*. The 132fsX mutant nullified anti-aggregate activity of the P299L CLN6 missense mutant but not of wild-type CLN6. Wild-type CLN6's resistance to the 132fsX mutant was abolished by replacement of amino acids 297–301, including Pro297 and Pro299, with five alanine residues. Given that removal of CLN6's C-terminal fifteen amino acids 297–311 (luminal tail) did not affect the resistance, we suggested that CLN6's luminal tail, when unleashed from Pro297/299-mediated conformational constraints, is improperly positioned by the 132fsX mutant, thereby blocking the induction of anti-aggregate activity. We here reveal a novel mechanism for dissipating CLN6 mutants' residual functions, providing an explanation for the compound heterozygosity-driven pathogenesis.

INTRODUCTION

CLN6 (Ceroid Lipofuscinosis, Neuronal, 6) is an endoplasmic reticulum (ER) protein and contains an N-terminal cytoplasmic domain, seven putative transmembrane domains, and a luminal C-terminus (Gao *et al.* 2002; Wheeler *et al.* 2002). Mutations in *CLN6* are linked to the development of CLN6 disease, one type of the neuronal ceroid lipofuscinoses (NCLs), a group of hereditary neurodegenerative disorders comprised of thirteen distinct types (Kollmann *et al.* 2013; Palmer *et al.* 2013; Warrier *et al.* 2013; Cárcel-Trullols *et al.* 2015; Mole *et al.* 2019; Butz *et al.* 2020; Nelvagal *et al.* 2020). CLN6 disease is characterized by seizures, motor difficulties, visual failure, and a shortened life-span, and is heterogeneous clinically and genetically, implying that CLN6's functionality is differentially impaired among patients (Alroy *et al.* 2011). CLN6's functions have been poorly understood, thereby making it difficult to assess the impacts of mutations in *CLN6*.

We previously showed that tethering the small

Address correspondence to: Dr. Tetsuo Yamazaki, Department of Molecular Cell Biology and Medicine, Graduate School of Biomedical Sciences, Tokushima University, 1-78-1, Sho-machi, Tokushima 770-8505, Japan
Tel: +81-88-633-7886, Fax: +81-88-633-9550
E-mail: tyamazak@tokushima-u.ac.jp (T. Yamazaki)

heat shock protein αB-crystallin (αBC), which otherwise is widely distributed throughout the cytoplasm, to the ER membrane suppresses aggregation of the myopathy-causing R120G αBC missense mutant (Yamamoto *et al.* 2014), highly prone to aggregate even when transfected into cell lines (Vicart *et al.* 1998). Subsequently, we isolated CLN6 as a binder to the ER-tethered αBC and revealed that CLN6 can prevent the R120G αBC mutant from aggregating. These findings indicated that the R120G αBC mutant serves as a model protein in determining the anti-aggregate activity of CLN6 and its mutants. Indeed, we demonstrated by employing the R120G αBC mutant that CLN6's anti-aggregate activity is compromised to various extents depending on which pathogenic mutation is introduced into *CLN6* (Yamashita *et al.* 2017, 2020). The finding led us to propose that the difference in functionality among CLN6 mutants can be assessed based on their anti-aggregate activity. We have so far analyzed anti-aggregate activity in a cell line transfected with a single CLN6 mutant. The activity detected is most likely to correlate with that in a patient homozygous for the corresponding CLN6 mutant. On the other hand, in order to predict what happens in patients compound heterozygous for CLN6 mutants, the overall activity exhibited by two different CLN6 mutants, but not the activity of each mutant, is required to be investigated.

In this study, we show that the anti-aggregate activity of one CLN6 mutant can be nullified by another mutant, pointing to functional interference between CLN6 mutants as the pathomechanisms operating in patients with CLN6 compound heterozygosity. Our findings have provided novel insight into the molecular basis of clinical and genetic heterogeneity of CLN6 disease.

MATERIALS AND METHODS

Expression vectors. The construction of pEGFP-N1-R120G αBC mutant (R120G αBC), pcDNA4/Myc-wild-type CLN6 (WT) and DNA4/Myc-R106PfsX26 CLN6 mutant (106fsX) was described previously (Yamamoto *et al.* 2014; Yamashita *et al.* 2017, 2020). The DNA fragment corresponding to the S132CfsX18, D173EfsX33, F239PfsX29 and A243PfsX26 CLN6 frameshift mutants (hereafter referred to as 132fsX, 173fsX, 239fsX and 243fsX, respectively) were generated by sequential PCRs. The first-step PCR was conducted using PrimeSTAR Mutagenesis Basal Kit (TAKARA Bio) with the pcDNA4/Myc-wild-type CLN6 as a template in combination with primers, named "Fwd" and "Rev" (Supporting Table 1). The PCR products were used as a template for the second-step PCR with following primers sets, "132fsX", "173fsX", "239fsX" and "243fsX" (Supporting Table 2). Other Myc-tagged CLN6 mutants were generated with the pcDNA4/Myc-wild-type CLN6 as a template in combination with primers described in Supporting Table 3. All the constructs were subjected to DNA sequencing. To generate pFLAG-CMV-5.1-wild-type CLN6 (CLN6-FLAG) and pFLAG-CMV-5.1-P299L CLN6 mutant (P299L-FLAG), pcDNA4/Myc-wild-type CLN6 or pcDNA4/myc-P299L CLN6 mutant were digested with HindIII/EcoRI and cloned in frame into the HindIII/EcoRI-digested pFLAG-CMV-5.1 (Sigma-Aldrich).

Cell culture and transfection. HeLa cells were maintained in Dulbecco's Modified Eagle Medium (nacalai tesque, Japan) supplemented with 10% fetal bovine serum at 37°C in a humidified cell culture incubator with 5% CO_2. For transfection experiments in 24-well plates, 1.5×10^4 HeLa cells were seeded per well in 0.5 mL of the cell growth medium 20 h before transfection. The cells in each well were transfected with 1.2 μL of Polyethylenimine (PEI) "Max" (Polysciences) mixed with 0.4 μg of single or multiple expression plasmids, where 0.2 μg each of two plasmids or 0.13 μg each of three plasmids were used. The transfection efficiency under these conditions was approximately 80% in all experiments.

Immunoblotting assays. At 16 h post-transfection, HeLa cells were lysed with 1 × Laemmli sample buffer (0.5 mM Tris-HCl (pH 6.8), 1.25% SDS, 12.5% glycerol, 1.25% 2-mercaptoethanol and 2.5% bromophenol blue), then centrifuged at 14,800 rpm for 5 min. The supernatant was collected, heated at 95°C for 1 min, resolved by SDS-PAGE, and electrotransferred onto polyvinylidene difluoride membranes. Then, the membranes were incubated with antibodies against Actin (1 : 200 diluted; Santa Cruz Biotechnology, C-2, sc-8432) or Myc (1 : 200 diluted; Santa Cruz Biotechnology, 9E10, sc-40) or FLAG (1 : 4500 diluted; Cell Signaling Technology) for 8 h at 4°C. Afterwards, the membranes were incubated for 20 min with horseradish peroxidase (HRP)-conjugated antibodies (1 : 8000 diluted; rabbit anti-mouse IgG, DAKO or 1 : 8000 diluted; goat anti-rabbit IgG, DAKO). HRP on the membrane was detected using the ECL Advance luminescence solution (GE Healthcare Life Science) according to the manufacturer's instruction.

Immunoprecipitation assays. HeLa cells were solubilized in lysis buffer (50 mM Tris (pH 8.0), 150 mM NaCl, 1% Nonidet P40 (NP-40), and protease inhibitor cocktail). Anti-FLAG antibody (Cell Signaling Technology) was added in the lysates and incubated for 15 min, and then protein A-Sepharose (GE Healthcare Life Sciences) was added and mixed by rotation for 15 min. Afterwards, protein A-Sepharose was collected and washed three times with lysis buffer. Finally, 2 × Laemmli sample buffer was added in the samples and heated at 95°C for 1 min.

Measurement of aggregate positivity. To visualize the EGFP-tagged R120G αBC missense mutant, a fluorescence microscope IX-51 (Olympus, Japan) with 20×/0.40 NA dry objective was used. At 16 h post-transfection, HeLa cells expressing EGFP-tagged R120G αBC mutants were illuminated with the mercury light (U-LH100HGAPO). EGFP images were captured with a digital camera WRAYCAM-SR300 (WRAYMER, Japan) and WraySpect (WRAYMER, Japan). WRAYCAM-SR300 was used through 0.35×c-mount lens. The EGFP-tagged R120G αBC mutant was observed as speckles of various size or as a diffuse signal widely distributed throughout the cytoplasm. A cell with speckle(s) was counted as an aggregate-positive cell, regardless of how large a speckle is and of how many speckles are found in the cell. The proportion of the aggregate-positive cells to the EGFP-positive cells was calculated and is shown as "Cells with aggregates (%)." At least 800 cells were analyzed for each condition in every assay.

Statistical analysis. All data are expressed as means ± S.E.M. The data was accumulated under each condition from at least five independent experiments. For parametric all-pairs multiple comparisons in all figures, Tukey-test was used.

RESULTS

The 132fsX truncated mutant was unable to prevent the R120G αBC mutant's aggregation

CLN6 disease is heterogeneous clinically and genetically (Cannelli *et al.* 2009; Chin *et al.* 2019). In order to investigate if the disease heterogeneity is associated with dysregulation of CLN6's anti-aggregate activity, we focused on the 132fsX prematurely terminated protein (Fig. 1A), which arises from a 2-bp deletion (c.395–396delCT), the most common mutation in *CLN6*, and corresponds to amino acids 1–131 of CLN6 followed by an irrelevant 18-amino acid stretch (Wheeler *et al.* 2002). Not only patients homozygous for the 132fsX mutant but also those compound heterozygous for this mutant have been described, among whom clinical manifestations are not consistent (Wheeler *et al.* 2002; Cannelli *et al.* 2009). Structurally, the 132fsX mutant lacks CLN6's third loop and beyond, the region required for CLN6's anti-aggregate activity (Yamashita *et al.* 2020). Collectively, the 132fsX mutant was expected to serve as an ideal tool with which to further explore the relationship between the disease heterogeneity and the reduction in CLN6's anti-aggregate activity. We first determined if the 132fsX mutant suppresses aggregation of the R120G disease-causing αBC mutant, a model protein highly prone to aggregate. When transfected into HeLa cells, the EGFP-tagged R120G αBC mutant was visualized as a diffuse signal widely distributed throughout the cytoplasm (the mutant spared from aggregation) or as intracellular speckles (the aggregated mutant) (Yamamoto *et al.* 2014). Based on microscopic images, we calculated the proportion of aggregate-positive cells to EGFP-positive cells. Transfection of Myc-tagged wild-type CLN6 into HeLa cells lowered aggregate positivity by ~15% compared with controls employing the insertless vector expressing Myc alone (Fig. 1B–D). In contrast, the percentage of aggregate-positive cells was not significantly affected upon transfection of the Myc-tagged 132fsX mutant, suggesting that the mutant lacks anti-aggregate activity.

The 132fsX mutant nullified anti-aggregate activity of coexisting CLN6 mutants

The 132fsX mutant-involving compound heterozygosity has been reported in four patients (Cannelli *et al.* 2009). Two of them have the 239fsX prematurely terminated protein, which arises from a 4-bp deletion (c.715–718delTTCG) and corresponds to amino acids 1–238 of CLN6 followed by an irrelevant 29-amino acid stretch (Cannelli *et al.* 2009) and the 132fsX truncated mutant, and the other two the P299L CLN6 missense mutant (Sharp *et al.* 2003) and the 132fsX truncated mutant (Fig. 2A). Meanwhile, the 106fsX truncated mutant, which corresponds to amino acids 1–105 of CLN6 followed by an irrelevant 26-amino acid stretch (Wheeler *et al.* 2002), has been found only in homozygous patients (Fig. 2A). The 1-bp insertion (c.316insC) producing the 106fsX prematurely terminated protein is identical to that in the *nclf* mouse, a naturally-occurring mouse model of CLN6 disease (Bronson *et al.* 1998; Gao *et al.* 2002; Wheeler *et al.* 2002; Kurze

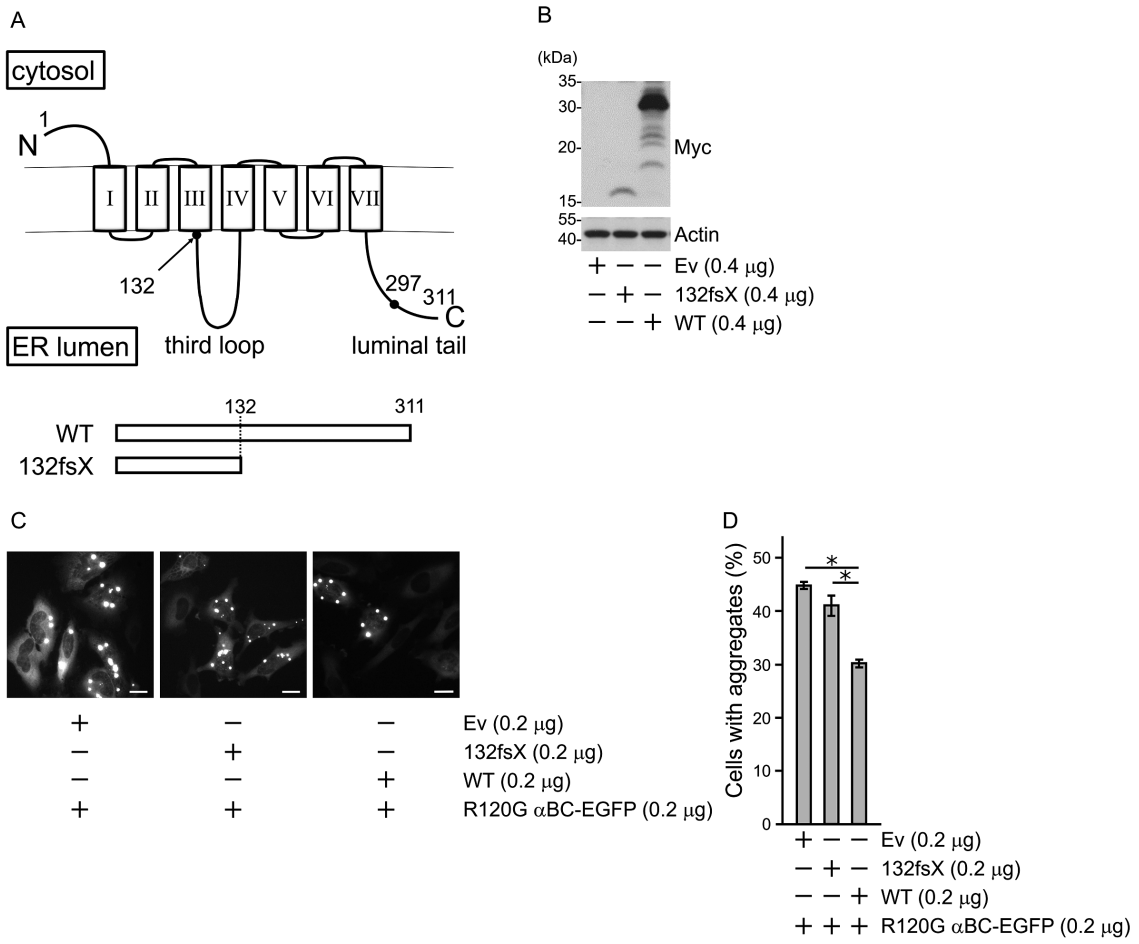

Fig. 1 The inability of the 132fsX mutant to prevent the R120G αBC mutant's aggregation. (**A**) Schematic representation of wild-type CLN6 (WT) and the 132fsX mutant. (**B**) HeLa cells were transfected with 0.4 μg each of the insertless vector (Ev), the Myc-tagged 132fsX mutant (132fsX)- or Myc-tagged wild-type CLN6 (WT)-expressing vector. The cells were lyzed 16 h after transfection. Their lysates were separated by SDS-PAGE and electrotransferred to PVDF membranes for the subsequent immunoblot analysis using the indicated antibodies. (**C**) HeLa cells were cotransfected with 0.2 μg of the expression construct encoding the EGFP-tagged R120G αBC mutant (R120G αBC-EGFP) in combination with 0.2 μg of either Ev, 132fsX- or WT-expressing vector. At 16 h post-transfection, the cells were examined by fluorescence microscopy to visualize the EGFP-tagged R120G αBC mutant. Shown are the images captured at this time point, where the EGFP-tagged R120G αBC mutant is observed as speckles of various size (aggregated) or as a diffuse signal widely distributed across the cytoplasm (spared from aggregation). Scale bars: 20 μm. (**D**) Based on the images in (C), a cell with speckle(s) was counted as an aggregate-positive cell, regardless of how large a speckle is and of how many speckles are found in the cell. The proportion of the aggregate-positive cells to the EGFP-positive cells was calculated and is shown as "Cells with aggregates (%)." At least 800 cells were analyzed for each condition in every assay. The data represent mean ± SEM of at least six independent experiments. * $P < 0.05$.

et al. 2010). We previously demonstrated that the 106fsX truncated mutant is unable to prevent the R120G αBC mutant from aggregating (Yamashita *et al.* 2020). In contrast with the 106fsX mutant, both the 239fsX and the P299L mutants inhibited the R120G αBC mutant's aggregation comparably to wild-type CLN6 (Fig. 2B, C). The finding prompted us to assess if their anti-aggregate activity is affected by simultaneous expression of the 132fsX mutant. Aggregate positivity in HeLa cells transfected with the 239fsX and the 132fsX mutants was ~15% higher than that in the cells transfected with the 239fsX mutant alone (Fig. 2D). Likewise, the P299L mutant's anti-aggregate activity was attenuated upon coexpression of the 132fsX mutant. Both the 239fsX and the P299L mutants were similarly disabled by the 106fsX truncated mutant. Given that wild-type CLN6's activity toward the R120G αBC mutant was not negatively impacted by the 106fsX or the 132fsX mutant (Fig. 2D), we suggested that these mutants

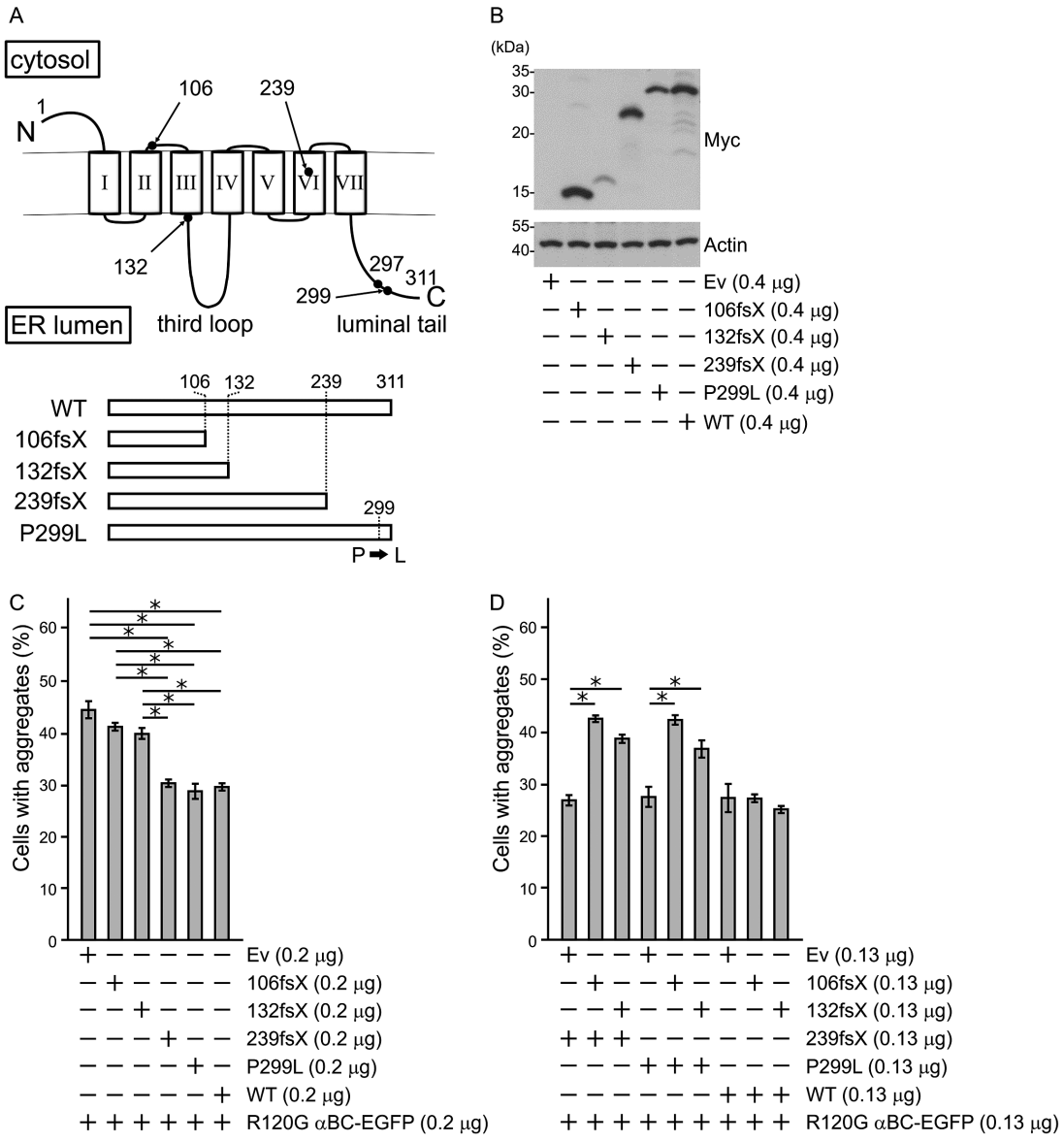

Fig. 2 Disruption by the 132fsX mutant of anti-aggregate activity of both the 239fsX and the P299L mutants. (**A**) Schematic representation of wild-type CLN6 (WT) and its mutants. (**B**) Immunoblot analysis performed as in Fig. 1(B). (**C** and **D**) Cells were transfected with the indicated combinations and amounts of expression vectors, and analyzed as in Fig. 1(C, D). The data represent mean ± SEM of six independent experiments. * $P < 0.05$.

lacking CLN6's third loop and beyond specifically counteract the coexisting CLN6 mutants.

The P299L mutant was selectively vulnerable to the 132fsX truncated mutant

In CLN6 disease patients, the 239fsX mutant has been described solely in combination with the 132fsX mutant. On the other hand, the P299L mutant has been found together with the 132fsX, the 173fsX, or the 243fsX mutant (Fig. 3A) (Cannelli *et al.* 2009; Kousi *et al.* 2012). Both the 173fsX and the 243fsX mutants are prematurely terminated proteins; the former arises from a 1-bp deletion (c.519delT) and corresponds to amino acids 1–172 of CLN6 followed by an irrelevant 33-amino acid stretch, and the latter arises from a 1-bp deletion (c.727delG) and corresponds to amino acids 1–242 of CLN6 followed by an irrelevant 26-amino acid stretch. We thus investigated if these three truncated mutants differentially affect the P299L mutant's anti-aggregate activity. The P299L mutant, when expressed alone, suppressed the R120G αBC mutant's aggre-

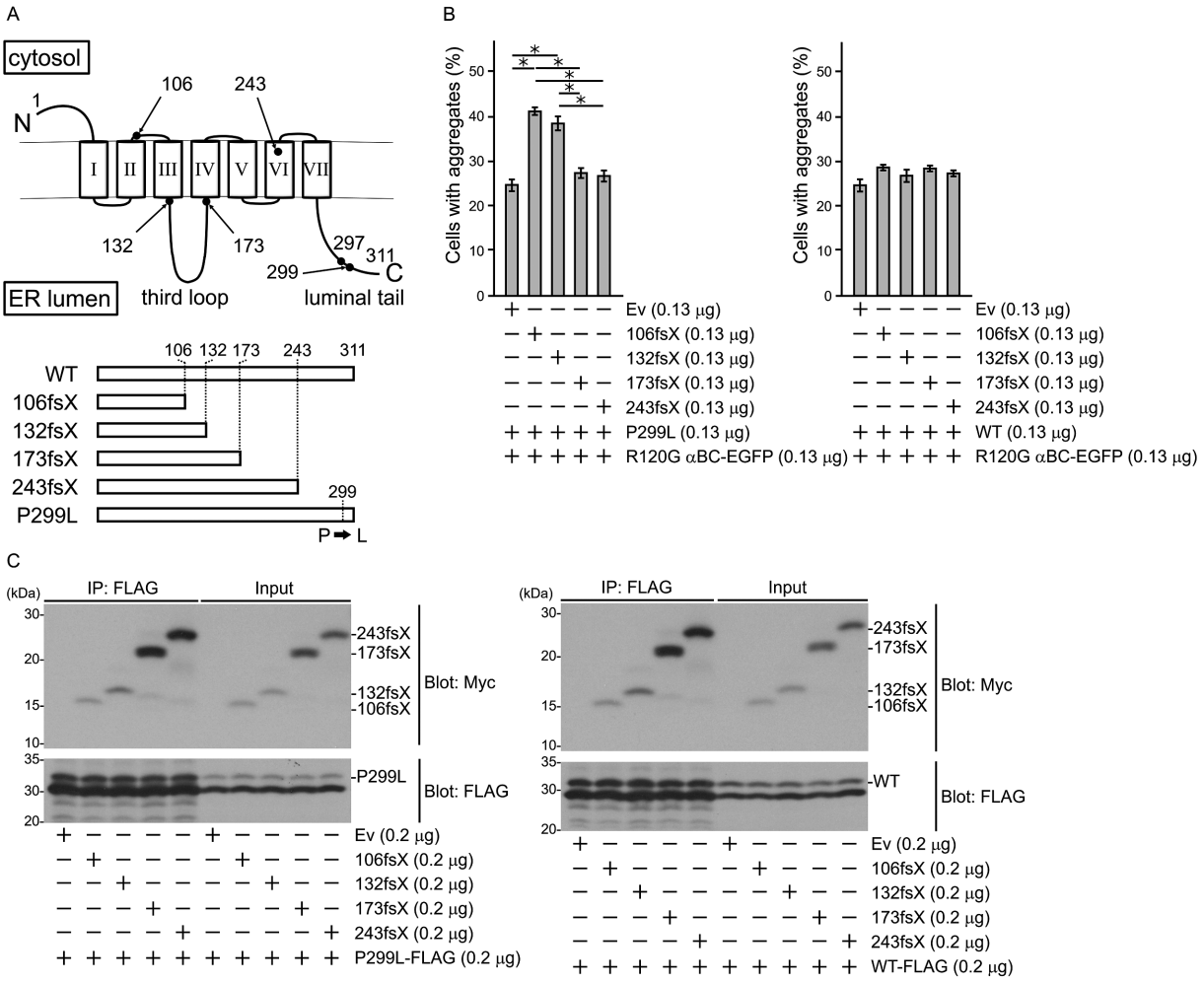

Fig. 3 The P299L mutant was disabled specifically by truncated mutants lacking CLN6's third loop and beyond. (**A**) Schematic representation of wild-type CLN6 (WT) and its mutants. (**B**) Cells were transfected with the indicated combinations and amounts of expression vectors, and analyzed as in Fig. 1(C, D). The data represent mean ± SEM of six independent experiments. * $P < 0.05$. (**C**) Cells were transfected with 0.2 μg of the FLAG-tagged P299L mutant (P299L-FLAG) or FLAG-tagged wild-type CLN6 (WT-FLAG) in combination with 0.2 μg of the indicated Myc-tagged CLN6 truncated mutant. The whole cell lysates (Input) and the FLAG immunoprecipitates (IP: FLAG) were immunoblotted using antibodies against Myc or FLAG.

gation, as shown by aggregate positivity of ~25% (Fig. 3B; Ev). The positivity was elevated by coexpression of the 106fsX or the 132fsX mutants, but not of the 173fsX or the 243fsX mutant. We thus reasoned that the P299L mutant is compromised only by truncated mutants that can physically interact with the P299L mutant. This was not the case in fact. Coimmunoprecipitation assays showed that every single truncated mutant employed here binds not only to the P299L mutant but also to wild-type CLN6 (Fig. 3C). Taken together, we suggested that the P299L mutant is disabled preferentially by truncated mutants lacking CLN6's third loop and beyond.

Integrity of CLN6's amino acids 297–301 was required to resist the 132fsX mutant

The importance of proline in protein structure is widely accepted (DeTar *et al.* 1977). Given that mutations of Pro297 and Pro299 in CLN6 have been described in patients (Sharp *et al.* 2003; Kousi *et al.* 2012), these proline residues would serve to ensure CLN6's structural integrity and consequently contribute to protection against the 132fsX mutant. We thus explored this idea by replacing amino acids 297–301 in CLN6 with five alanine residues (Fig. 4A; 5A1). The 5A1 mutant, when expressed alone, suppressed the R120G αBC mutant's aggregation (Fig. 4B, C). Its anti-aggregate activity, however, was attenuated

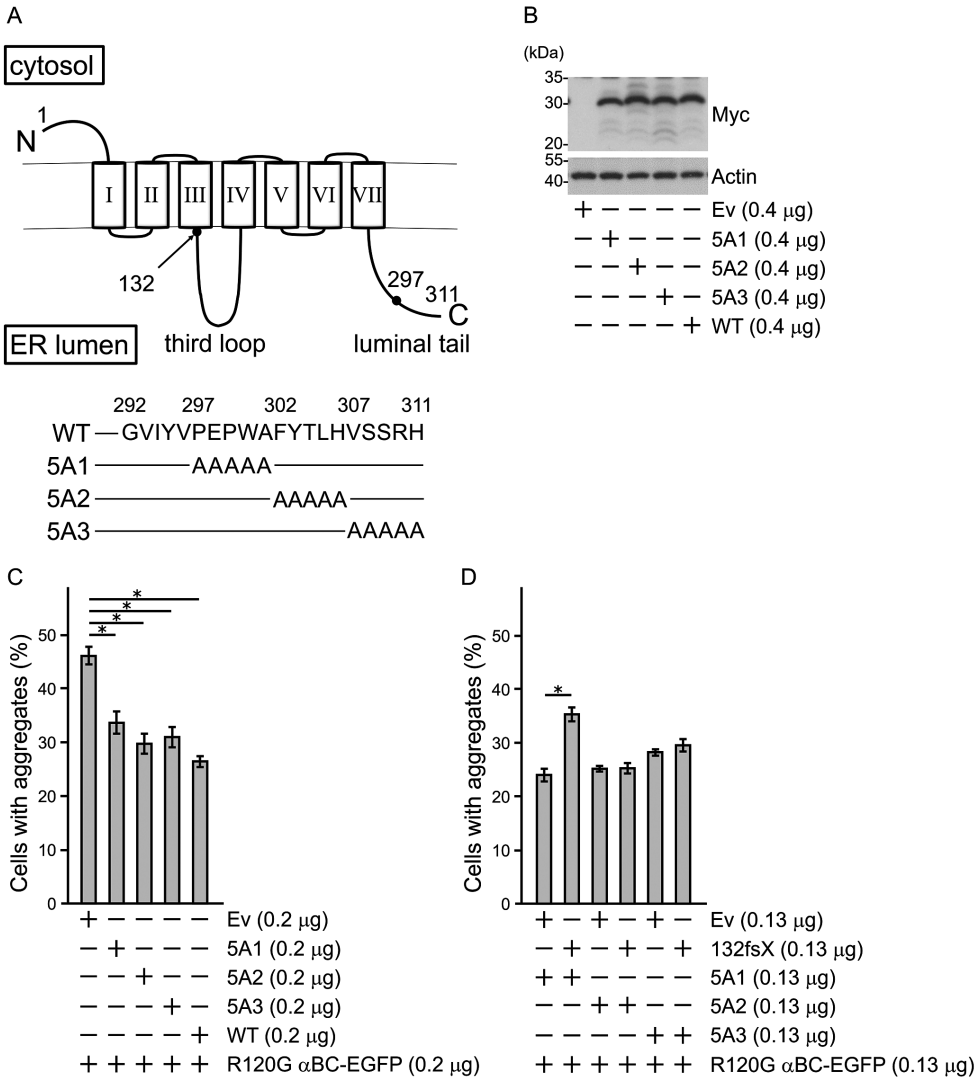

Fig. 4 Integrity of CLN6's amino acids 297–301 conferred resistance to the 132fsX mutant. (**A**) Schematic representation of wild-type CLN6 (WT) and its mutants. (**B**) Immunoblot analysis performed as in Fig. 1(B). (**C** and **D**) Cells were transfected with the indicated combinations and amounts of expression vectors, and analyzed as in Fig. 1(C, D). The data represent mean ± SEM of six independent experiments. * $P < 0.05$.

by the simultaneously expressed 132fsX mutant (Fig. 4D). In contrast, CLN6 mutants with the rest of the luminal tail replaced with alanine residues (Fig. 4A; 5A2 and 5A3) were refractory to the 132fsX-mediated suppression (Fig. 4B–D), indicating that the amino acids 297–301 are key to CLN6's resistance to the 132fsX mutant.

Removal of CLN6's luminal tail resulted in insensitivity to the 132fsX mutant

The mutational analysis noted above led us to hypothesize that when unleashed from structural constraints imposed by the amino acids 297–301, CLN6's luminal tail (amino acids 297–311) is improperly positioned by the 132fsX mutant, thereby causing a failure to exert anti-aggregate activity. We thus tested our hypothesis using a CLN6 mutant lacking amino acids 297–311 (Fig. 5A; P297X). The P297X mutant not only displayed anti-aggregate activity comparably to wild-type CLN6 but also was resistant to the coexisting 132fsX mutant (Fig. 5B–D), arguing for our hypothesis. Collectively, we suggested that a loss of a tight structural control over CLN6's luminal tail underlies the vulnerability to the 132fsX mutant.

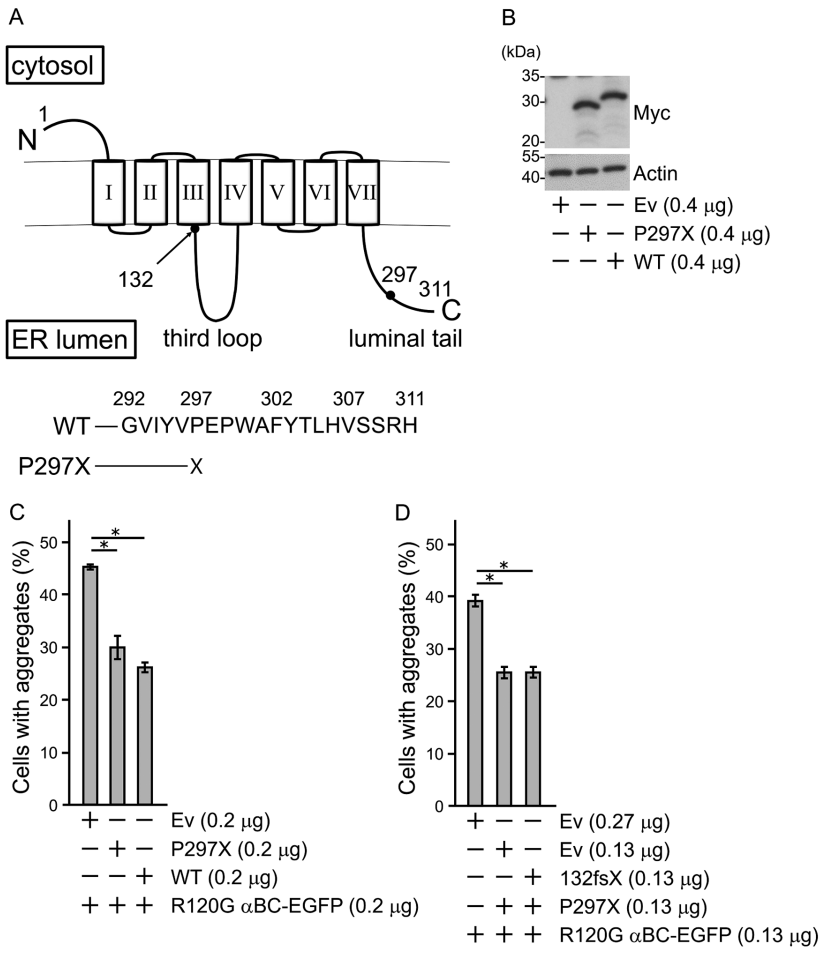

Fig. 5 Removal of CLN6's luminal tail resulted in insensitivity to the 132fsX mutant. (**A**) Schematic representation of wild-type CLN6 (WT) and the P297X mutant. (**B**) Immunoblot analysis performed as in Fig. 1(B). (**C** and **D**) Cells were transfected with the indicated combinations and amounts of expression vectors, and analyzed as in Fig. 1(C, D). The data represent mean ± SEM of six independent experiments. * $P < 0.05$.

DISCUSSION

Both the P299L and the 5A1 mutants, when expressed alone, prevented aggregation of the R120G αBC mutant. These mutants' anti-aggregate activity was, however, offset by the simultaneously expressed 132fsX mutant. Meanwhile, wild-type CLN6 was not affected by the 132fsX mutant, indicating that integrity of CLN6's amino acids 297–301 is vital to resisting the 132fsX mutant-driven interference. The importance of this five-amino-acid stretch is also supported by genetic findings in patients. Within CLN6's C-terminal thirty amino acids (282–311), which follow the seventh transmembrane domain and face the ER lumen, six mutations have been found. All except one accumulate within amino acids 297–301: Pro297Thr, Pro297LeufsX, Glu298Lys, Pro299Leu, and Trp300Arg (Sharp *et al.* 2003; Teixeira *et al.* 2003; Arsov *et al.* 2011; Kousi *et al.* 2012; Sun *et al.* 2018). It should be noted that mutations at both Pro297 and Pro299 have been found in patients. The critical role that proline plays for protein structure has been well known (DeTar *et al.* 1977; Jing *et al.* 1998; Newbold *et al.* 2001). In contrast, the extent to which amino acid residues other than proline contribute to protein structure is not generalized. We expected that what the amino acids 297–301 provide is a structural basis for CLN6's functionality, which would be established chiefly by Pro297 and Pro299. Indeed, the P299L and the 5A1 mutants, when coexpressed with the 132fsX, became unable to display their intrinsic anti-aggregate activity, arguing for our idea. Furthermore, the P297X mutant, which lacks CLN6's luminal tail (amino acids 297–311), exerted its anti-aggregate activity either with or without the 132fsX

mutant. We therefore suggested that CLN6's luminal tail needs to be properly positioned for CLN6 to display its anti-aggregate activity and that the spatial constraint imposed on the tail is provided chiefly by Pro297 and Pro299. Of note, the P299L mutant was not disabled by the 173fsX or the 243fsX mutant. It would be that these two truncated mutants, unlike the 132fsX mutant, shield the P299L mutant's region responsible for its anti-aggregate activity from access of its luminal tail. Meanwhile, the 239fsX mutant was compromised by the coexpressed 132fsX mutant despite the lack of the stretch of amino acids corresponding to CLN6's luminal tail. It might be that an exquisite arrangement of seven transmembrane segments is indispensable for CLN6's structural stability. Considering that Phe239 is predicted to be in the middle of CLN6's sixth transmembrane segment (Sharp *et al.* 2003), the 239fsX mutant would be less rigid relative to wild-type CLN6. In consequence, the 132fsX mutant is likely to disturb the 239fsX mutant's structure, thereby nullifying its anti-aggregate activity. Recently, a homozygous mutation in cat CLN6 has been reported, where a guanine to adenine change (c.668G>A) creates a termination codon at Trp 223 (pTrp223Ter) (Katz *et al.* 2020). Like human CLN6, cat CLN6 is also predicted to have seven transmembrane domains based on TMHMM, a membrane protein topology prediction program (http://www.cbs.dtu.dk/services/TMHMM/) and the Trp223 is situated in the fifth transmembrane domain (Supporting Fig. 1). A cat homozygous for the c.668G>A mutation displayed clinical signs characteristic of the neuronal ceroid lipofuscinoses, revealing that the protein product pTrp223Ter is a loss-of-function CLN6 mutant. Given that the 239fsX human CLN6 mutant is prematurely terminated in the sixth transmembrane domain, a perturbation in CLN6 transmembrane domains is likely to affect the entire structure of CLN6 and in turn to impair its functionality.

The third loop, predicted to face the ER lumen and also referred to as the second luminal loop, of CLN6 has been associated with ER-to-Golgi trafficking of a spectrum of lysosomal enzymes (Bajaj *et al.* 2020). We previously demonstrated the requirement for the third loop in CLN6's anti-aggregate activity (Yamashita *et al.* 2020). Based on the dysfunctionality of the pTrp223Ter cat CLN6 mutant (Katz *et al.* 2020) and the vulnerability of the 239fsX human CLN6 mutant to the 132fsX truncated mutant, the presence of the third loop itself is necessary but not sufficient for the full-fledged activity of CLN6. It might be that a premature termination within CLN6's transmembrane domains results in the disruption of an exquisite spatial arrangement of each domain, thereby altering the third loop's structure.

We have demonstrated that the 132fsX mutant offsets the 239fsX and the P299L mutants' suppressive effect on the R120G αBC mutant's aggregation, and that neither the 173fsX nor the 243fsX mutant exhibits such compromising activity, proposing that clinical outcomes of patients compound heterozygous for the 132fsX mutant and either the 239fsX or the P299L mutant are attributable to the loss of anti-aggregate activity. On the other hand, symptoms of patients with either homozygosity for the P299L mutant or compound heterozygosity for the P299L mutant and the 173fsX or the 243fsX mutant might be explained by CLN6's functional defects unrelated to its anti-aggregate activity. Alternatively, the clinical manifestations of this group of patients would be ascribed to aggregation of CLN6's physiological targets. A caveat is that what we have determined so far is anti-aggregate activity toward the R120G αBC mutant, a model protein, but not that toward CLN6's physiological target proteins. Therefore, the prevention of the R120G αBC mutant's aggregation validated in HeLa cells transfected with the P299L mutant alone or together with the 173fsX or the 243fsX mutant, does not necessarily mean that every single CLN6's physiological target is safeguarded against aggregation-inducing insults in patients harboring the P299L mutant alone or together with the 173fsX or the 243fsX mutant. We hence expect that the spectrum of CLN6's physiological targets remaining functional is different from patient to patient depending on which mutant or combination of CLN6 mutants each patient has, thereby giving rise to the symptom disparity. Patients with compound heterozygosity for the P299L and the 173fsX mutants have been reported to present with visual impairment, a characteristic feature of late infantile-onset CLN6 disease, whereas those with homozygosity for the P299L mutant not (Cannelli *et al.* 2009), arguing for our idea.

Here we propose that the functional interference between coexisting CLN6 mutants is implicated in the development of CLN6 disease. Our findings provide novel insight into pathogenic mechanisms operating in patients with compound heterozygosity for CLN6 mutants.

Acknowledgements

This work was supported by Japan Society for the

Promotion of Science (JSPS) KAKENHI Grant Numbers JP18K07045 (T. Y.) and JP16J09784 (A. Y.), and the Tokushima Shimbun Science Grant (Y. S.).

CONFLICT OF INTEREST

The authors have no conflicts of interest to declare.

REFERENCES

Alroy J, Braulke T, Cismondi IA, Cooper JD, Creegan D, *et al.* (2011) CLN6. in *Neuronal Ceroid Lipofuscinoses (Batten Disease)* (ed. by Mole SE *et al.*) pp159–175, Oxford University Press.

Arsov T, Smith KR, Damiano J, Franceschetti S, Canafoglia L, *et al.* (2011) Kufs disease, the major adult form of neuronal ceroid lipofuscinosis, caused by mutations in cln6. *Am J Hum Genet* **88**, 566–573.

Bajaj L, Sharma J, di Ronza A, Zhang P, Eblimit A, *et al.* (2020) A CLN6-CLN8 complex recruits lysosomal enzymes at the ER for Golgi transfer. *J Clin Invest* **140**, 4118–4132.

Bronson RT, Donahue LR, Johnson KR, Tanner A, Lane PW, *et al.* (1998) Neuronal ceroid lipofuscinosis (nclf), a new disorder of the mouse linked to chromosome 9. *Am J Med Genet* **77**, 289–297.

Butz ES, Chandrachud U, Mole SE and Cotman SL (2020) Moving towards a new era of genomics in the neuronal ceroid lipofuscinoses. *Biochim Biophys Acta – Mol Basis Dis* **1866**, 165571.

Cannelli N, Garavaglia B, Simonati A, Aiello C, Barzaghi C, *et al.* (2009) Variant late infantile ceroid lipofuscinoses associated with novel mutations in CLN6. *Biochem Biophys Res Commun* **379**, 892–897.

Cárcel-Trullols J, Kovács AD and Pearce DA (2015) Cell biology of the NCL proteins: What they do and don't do. *Biochim Biophys Acta – Mol Basis Dis* **1852**, 2242–2255.

Chin JJ, Behnam B, Davids M, Sharma P, Zein WM, *et al.* (2019) Novel mutations in CLN6 cause late-infantile neuronal ceroid lipofuscinosis without visual impairment in two unrelated patients. *Mol Genet Metab* **126**, 188–195.

DeTar DLF and Luthra NP (1977) Conformations of Proline. *J Am Chem Soc* **99**, 1232–1244.

Gao H, Boustany RMN, Espinola JA, Cotman SL, Srinidhi L, *et al.* (2002) Mutations in a novel CLN6-encoded transmembrane protein cause variant neuronal ceroid lipofuscinosis in man and mouse. *Am J Hum Genet* **70**, 324–335.

Heine C, Quitsch A, Storch S, Martin Y, Lonka L, *et al.* (2007) Topology and endoplasmic reticulum retention signals of the lysosomal storage disease-related membrane protein CLN6. *Mol Membr Biol* **24**, 74–87.

Jing PI, Dogovski C and Pittard AJ (1998) Functional consequences of changing proline residues in the phenylalanine-specific permease of Escherichia coli. *J Bacteriol* **180**, 5515–5519.

Katz ML, Buckley RM, Biegen V, O'Brien DP, Johnson GC, *et al.* (2020) Neuronal ceroid lipofuscinosis in a domestic cat associated with a DNA sequence variant that creates a premature stop codon in CLN6. *G3 Genes, Genomes, Genet* **10**, 2741–2751.

Kollmann K, Uusi-Rauva K, Scifo E, Tyynelä J, Jalanko A, *et al.* (2013) Cell biology and function of neuronal ceroid lipofuscinosis-related proteins. *Biochim Biophys Acta – Mol Basis Dis* **1832**, 1866–1881.

Kousi M, Lehesjoki AE and Mole SE (2012) Update of the mutation spectrum and clinical correlations of over 360 mutations in eight genes that underlie the neuronal ceroid lipofuscinoses. *Hum Mutat* **33**, 42–63.

Kurze AK, Galliciotti G, Heine C, Mole SE, Quitsch A, *et al.* (2010) Pathogenic mutations cause rapid degradation of lysosomal storage disease-related membrane protein CLN6. *Hum Mutat* **31**, E1163–1174.

Mole SE, Anderson G, Band HA, Berkovic SF, Cooper JD, *et al.* (2019) Clinical challenges and future therapeutic approaches for neuronal ceroid lipofuscinosis. *Lancet Neurol* **18**, 107–116.

Mole SE, Michaux G, Codlin S, Wheeler RB, Sharp JD, *et al.* (2004) CLN6, which is associated with a lysosomal storage disease, is an endoplasmic reticulum protein. *Exp Cell Res* **298**, 399–406.

Nelvagal HR, Lange J, Takahashi K, Tarczyluk-Wells MA and Cooper JD (2020) Pathomechanisms in the neuronal ceroid lipofuscinoses. *Biochim Biophys Acta – Mol Basis Dis* **1866**, 165570.

Newbold RJ, Deery EC, Walker CE, Wilkie SE, Srinivasan N, *et al.* (2001) The destabilization of human GCAP1 by a proline to leucine mutation might cause cone-rod dystrophy. *Hum Mol Genet* **10**, 47–54.

Palmer DN, Barry LA, Tyynelä J and Cooper JD (2013) NCL disease mechanisms. *Biochim Biophys Acta – Mol Basis Dis* **1832**, 1882–1893.

Sharp JD, Wheeler RB, Parker KA, Gardiner RM, Williams RE, *et al.* (2003) Spectrum of CLN6 mutations in variant late infantile neuronal ceroid lipofuscinosis. *Hum Mutat* **22**, 35–42.

Sun G, Yao F, Tian Z, Ma T and Yang Z (2018) A first CLN6 variant case of late infantile neuronal ceroid lipofuscinosis caused by a homozygous mutation in a boy from China: A case report. *BMC Med Genet* **19**, 177.

Teixeira CA, Espinola J, Huo L, Kohlschütter J, Sawin DAP, *et al.* (2003) Novel mutations in the CLN6 gene causing a variant late infantile neuronal ceroid lipofuscinosis. *Hum Mutat* **21**, 502–508.

Vicart P, Caron A, Guicheney P, Li Z, Prévost MC, *et al.* (1998) A missense mutation in the αb-crystallin chaperone gene causes a desmin-related myopathy. *Nat Genet* **20**, 92–95.

Warrier V, Vieira M and Mole SE (2013) Genetic basis and phenotypic correlations of the neuronal ceroid lipofusinoses. *Biochim Biophys Acta – Mol Basis Dis* **1832**, 1827–1830.

Wheeler RB, Sharp JD, Schultz RA, Joslin JM, Williams RE, *et al.* (2002) The gene mutated in variant late-infantile neuronal ceroid lipofuscinosis (CLN6) and in nclf mutant mice encodes a novel predicted transmembrane protein. *Am J Hum Genet* **70**, 537–542.

Yamamoto S, Yamashita A, Arakaki N, Nemoto H and Yamazaki T (2014) Prevention of aberrant protein aggregation by anchoring the molecular chaperone αb-crystallin to the endoplasmic reticulum. *Biochem Biophys Res Commun* **455**, 241–245.

Yamashita A, Hiraki Y and Yamazaki T (2017) Identification of CLN6 as a molecular entity of endoplasmic reticulum-driven anti-aggregate activity. *Biochem Biophys Res Commun* **487**, 917–922.

Yamashita A, Shiro Y, Hiraki Y, Yujiri T and Yamazaki T (2020) Implications of graded reductions in CLN6's anti-aggregate activity for the development of the neuronal ceroid lipofuscinoses. *Biochem Biophys Res Commun* **525**, 883–888.

Supporting Table 1 *Primers used for the first step of constructing expression vectors*

Target	Primer	Sequence
132fsX	395-396delCT-Fwd	5'-GGTGACTGTCAACCACCGCCTGCTC-3'
	395-396delCT-Rev	5'-TGGTTGACAGTCACCCACCAGGTGGA-3'
173fsX	519delT-Fwd	5'-ATTATGAGAGTACCTGGGTCACTGC-3'
	519delT-Rev	5'-AGGTACTCTCATAATAGTAGAGCAGC-3'
239fsX	715-718delTTCG-Fwd	5'-CACCTTCCCATGCTGGCCCTCGTCC-3'
	715-718delTTCG-Rev	5'-CAGCATGGGAAGGTGAAGATGAAGAG-3'
243fsX	727delG-Fwd	5'-CATGCTGCCCTCGTCCTGCACCAGA-3'
	727delG-Rev	5'-GACGAGGGCAGCATGGCGAAGAAGGT-3'

Supporting Table 2 *Primers used for the second step of constructing expression vectors*

Target	Sequence
132fsX	5'-CTGTCCGTGGAATTCTGCAGATATC-3'
	5'-GAATTCCACGGACAGACAGGTGGTGC-3'
173fsX	5'-GAGAGCTTGGAATTCTGCAGATATC-3'
	5'-GAATTCCAAGCTCTCAGCTTTAGAGG-3'
239fsX	5'-TTCGCACTGGAATTCTGCAGATATC-3'
	5'-GAATTCCAGTGCGAAGGAGGAGAAGA-3'
243fsX	5'-TTCGCACTGGAATTCTGCAGATATC-3'
	5'-GAATTCCAGTGCGAAGGAGGAGAAGA-3'

Supporting Table 3 *The following primers sets are used in generating the CLN6 mutants*

Target	Sequence
P299L	5'-CCTGAGCTCTGGGCATTCTACACCCT-3'
	5'-TGCCCAGAGCTCAGGGACGTAGATGA-3'
5A1	5'-CGCAGCAGCAGCAGCTTTCTACACCCTTCAC-3'
	5'-GCTGCTGCTGCTGCGACGTAGATGACACCCGG-3'
5A2	5'-GCAGCAGCAGCAGCAGTCAGCAGTCGGCACTGG-3'
	5'-TGCTGCTGCTGCTGCAGCCCAGGGCTCAGGGAC-3'
5A3	5'-GCAGCAGCAGCAGCATGGAATTCTGCAGATATC-3'
	5'-TGCTGCTGCTGCTGCGTGAAGGGTGTAGAAAGC-3'
P297X	5'-TACGTCCTGTGGAATTCTGCAGATATCCAGCAC-3'
	5'-ATTCCACAGGACGTAGATGACACCCGGGTACTTC-3'

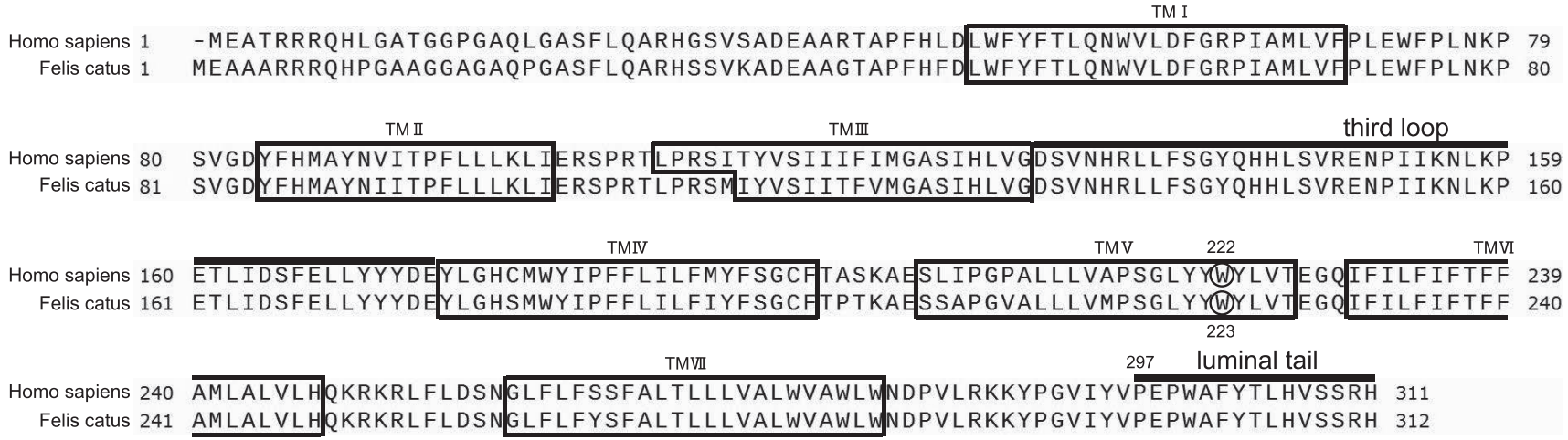

Supporting Fig. 1 Topological features shared by human and cat CLN6s. Boxed are transmembrane domains (TMs). Amino acids situated between the third (TM3) and the fourth (TM4) transmembrane domains correspond to the third loop.